The Aeronautical Journal (2023), **127**, pp. 1676–1697
doi:10.1017/aer.2023.26

REGULAR PAPER

Lift alleviation in travelling vortical gusts

Y. Qian , Z. Wang and I. Gursul*

University of Bath, Bath BA2 7AY, United Kingdom
*Corresponding author. Email: i.a.gursul@bath.ac.uk

Received: 9 January 2023; **Revised:** 6 March 2023; **Accepted:** 8 March 2023

Keywords: lift alleviation; mini-spoiler; gust; swept wing

Abstract

Lift alleviation by a mini-spoiler on aerofoils, unswept and swept wings encountering an isolated counter-clockwise vortical gust was investigated by means of force and velocity measurements. The flow separation region behind the spoiler remains little affected during the gust encounter. The maximum lift reduction is found for the static stall angle of attack. The change in the maximum lift during the gust encounter is approximately equal to that in steady freestream. The comparison with plunging aerofoils reveals that, for the same maximum gust and plunge velocity, the effectiveness of the mini-spoiler is much better in travelling gusts. This reveals the importance of the streamwise length scale of the incident gust. For the unswept wing, there is some three-dimensionality of the flow separation induced by the mini-spoiler near the wing tip. The magnitude of the lift reduction can be estimated using the aerofoil data and by making an aspect ratio correction for the reduced effective angle of attack. For the swept wing, the mini-spoiler can disrupt the formation of a leading-edge vortex induced by the incident vortex on the clean wing and can still reduce the maximum lift.

Nomenclature

LEV	leading-edge vortex
ND: YAG	neodymium-doped yttrium aluminium garnet
PIV	particle image velocimetry
V3V	volumetric 3-component velocimetry
a_0	slope of lift coefficient
AR	aspect ratio
c	chord length
h	mini-spoiler height
sAR	semi-aspect ratio
t	time
t_s	mini-spoiler thickness
w	velocity in z-direction
w'	spanwise velocity
x, y, z	streamwise and cross-stream coordinates
y_{VI}	vortex initial cross-stream location
y_{LE}	leading-edge cross-stream location
α	angle of attack
ε	normalised offset distance
ω	z-vorticity
C_L	lift coefficient
Q	Q-criterion
Re	chord Reynolds number
U_∞	freestream velocity
$V_{gust,\,max}$	maximum gust velocity

V_{max}	maximum tangential velocity of incident vortex
Γ	circulation of incident vortex
Λ	wing sweep angle

1.0 Introduction

Loads control on wings during gusts, turbulence, and manoeuvers may help design lighter wing structures, which could also help for drag reduction. Even quasi-steady lift changes can be substantial for large civil transport aircraft flying in turbulence (equivalent to peak-to-peak gust amplitudes of up to 3 degrees for cruise and 12 degrees at take-off and landing [1]) and for small air vehicles in the atmospheric boundary layers (up to 20 degrees [2]).

The theoretical unsteady aerodynamics of wings with attached flows in gusts predict that the amplitude of the unsteady lift decreases with the reduced frequency [3, 4]. This was confirmed by various experimental investigations when flow separation did not occur (see for example recent work [5–7]). However, with increasing angle of attack of the wing, incoming gusts may cause excursions to the post-stall regime in which well-known dynamic stall and larger lift hysteresis are observed [8]. Separated flows result in much larger lift changes than attached flows [7], if the gust causes the formation of a leading-edge vortex (LEV). The primary parameter that determines the maximum lift was found to be the maximum effective angle of attack rather than the reduced frequency or the reduced pitch rate [7] for the parameter range tested. Flow separation and LEV formation can occur for stationary wings in gusts, flexible wings with unsteady deformation and in manoeuvers.

Various types of gusts were generated in experimental facilities to study their interaction with wings. These include travelling-wave gusts, concentrated vortices, and standing-wave gusts. Periodic travelling-wave gusts were generated by oscillating aerofoils or cascade of aerofoils [6, 9–14] and by oscillating flaps [15, 16]. Concentrated vortices were also produced by pitching or plunging upstream aerofoils [11, 17–19]. Standing-wave gust generators work by the deflection of freestream and can be produced by oscillating two large side-by-side aerofoils or flaps to vary the direction of the freestream flow [20], oscillating the walls of the test section [21] and oscillating small fences on the wind tunnel walls [7].

The streamwise length scale (i.e. wavelength) of the gusts is typically large (corresponding to low reduced frequencies) for the travelling-wave gusts and is very large for the standing-wave gusts. The gust cross-stream length scale is also typically large compared to the aerofoil dimensions for both types of gust generators. In contrast, for concentrated single-vortex type of gusts, both the streamwise and cross-stream length scales are finite and may be on the same order or smaller than the chord length of the downstream aerofoil. This kind of vortical gusts represent more realistic cases with large but localised velocity fluctuations. This paper investigates lift attenuation for concentrated vortical gusts interacting with downstream wings. The vortical gusts were generated by using the methodology developed by Qian et al. [19]. The main advantage of the method is the capability of producing nearly two-dimensional vortex filaments with small core size, which allowed us to investigate the interaction with aerofoils, unswept and swept wings.

Traditional alleviation strategies (such as ailerons, flaps and spoilers) are not suitable for high-frequency actuation because of their large inertia. Search for high-frequency actuators focused on small spoilers (fences or tabs), which are typically smaller than 4% of the chord length [22–26], blowing as normal jets, counter-flowing wall-jets and upstream facing oblique jets [27–32] and bleed [33, 34]. The location of the actuation proved to be the most important parameter and changes the nature of the lift attenuation. Either fences or blowing near the trailing -edge mostly deflects the flow upwards while causing minor flow separation just upstream. Deflected flow is the mirror image of the flow of a traditional Gurney flap. The magnitude of the lift change decreases with increasing angle of attack as thicker boundary layer or weak separation develops near the actuator.

In contrast, mini-spoilers or counter-flowing wall jets near the leading edge cause forced separation, which approaches the Kirchhoff-Rayleigh flow in the limit. The biggest advantage of this approach is its much-reduced lift slope, which is highly desirable in turbulence and gust encounters. The magnitude of

https://doi.org/10.1017/aer.2023.26 Published online by Cambridge University Press

the lift decrease increases with angle of attack and is larger than that of the trailing-edge actuation. This paper investigates lift attenuation by using mini-spoilers (with normalised height $h/c = 0.04$) located near the leading edge (at $x/c = 0.08$) following our previous work with such device on an aerofoil in freestream in the absence of a gust [25, 26]. We investigate the lift attenuation for the vortical gusts generated by Qian et al. [19] using the mini-spoiler near the leading edge.

A second advantage of placing an actuator near the leading edge rather than the trailing edge is the capability of lift attenuation when flow separation and LEV formation is unavoidable. A mini-spoiler placed near the leading edge of a periodically plunging aerofoil has been shown to delay the roll-up of the shear layer and the formation of a LEV [35]. This becomes possible as the angle of attack is increased and when the unsteady effects (amplitude and frequency of the plunging motion) are not too large. The delay of the dynamic stall vortex by enforcing separation by a mini-spoiler may increase the drag temporarily, but the actuation is expected to be for a short duration only. For fixed-wing applications and wind turbine blades, the main objective is to reduce the bending moment; therefore, this method may be suitable. In contrast, for rotorcraft applications, the objectives are to reduce the pitching moment and to increase the cycle-averaged lift [36], which require application of flow control for long durations and many cycles. Consequently, previous dynamic stall control schemes focused on the delay of flow separation and LEV formation, using various methods including blowing, suction, plasma actuation and others [37–41]. We note that these active flow control methods may present practical challenges in the design of the wings. This paper focuses on mini-spoilers, which may be easier to implement for the fixed-wing applications. The rigid stationary wings in transient gusts are considered.

We investigated the lift attenuation by using a mini-spoiler near the leading edge of a rigid stationary wing. We studied an aerofoil, an unswept wing with finite aspect ratio and a swept wing. The nearly two-dimensional vortical gusts were generated upstream of the wings. The isolated vortical gusts had maximum vortex velocity on the order of the freestream velocity. The unsteady lift and velocity field were measured to understand the effects of the mini-spoiler during the gust-wing interaction.

2.0 Experimental methods

Experiments were conducted in a closed-loop water tunnel (The Eidetics model 1,520) located at the University of Bath. The vortical gusts were generated by using the set-up described by Qian et al. [19]. An upstream aerofoil was plunged with a transient motion (first rapidly and then slowly), which generated a single counter-clockwise vortex that travelled downstream with approximately freestream velocity. The two-dimensionality of the vortex was demonstrated by Qian et al. [19]. The plunging upstream aerofoil set at an angle of attack of zero degrees had a cross-section profile of NACA0012 and a chord length of $c = 62.7$ mm and was mounted vertically in the water tunnel as sketched in Fig. 1. The end plates were placed at both ends of the upstream aerofoil to maintain nominally two-dimensional flow. By varying the plunge amplitude, we were able to generate a weak vortex with a dimensionless circulation of $\Gamma/U_\infty c = 0.55$ and a strong vortex with a dimensionless circulation of $\Gamma/U_\infty c = 1.07$. The variation of the phase-averaged cross-stream velocity component across the vortex core is shown in Fig. 1(a) for the strong vortex, where r is the distance from the vortex centre. The vortex core radius is approximately $0.06c$. The corresponding maximum tangential velocity V_{max}/U_∞ was approximately 0.5 and 1.0 for the weak and strong vortex, respectively. Further details can be found in [19].

A downstream aerorfoil, a finite unswept wing, and a finite swept wing were placed downstream of the plunging aerofoil. The three models are shown in Fig. 1(b). The origin is at the final cross-stream location of the trailing edge of the upstream aerofoil. The streamwise coordinate is x, the cross-stream coordinate is y, the spanwise coordinate is z, and $z = 0$ corresponds to the root of the downstream wing. The downstream aerofoil and finite wings had a cross-section profile of NACA 0012 and the same chord length of $c = 62.7$ mm. The half-models were mounted vertically. Both the unswept ($\Lambda = 0°$) and the swept ($\Lambda = 40°$) downstream wings had a semi-aspect ratio of $sAR = 3$. For the case of the downstream aerofoil, an additional end plate was placed. All cases were tested at a chord Reynolds number of $Re = 2 \times 10^4$.

https://doi.org/10.1017/aer.2023.26 Published online by Cambridge University Press

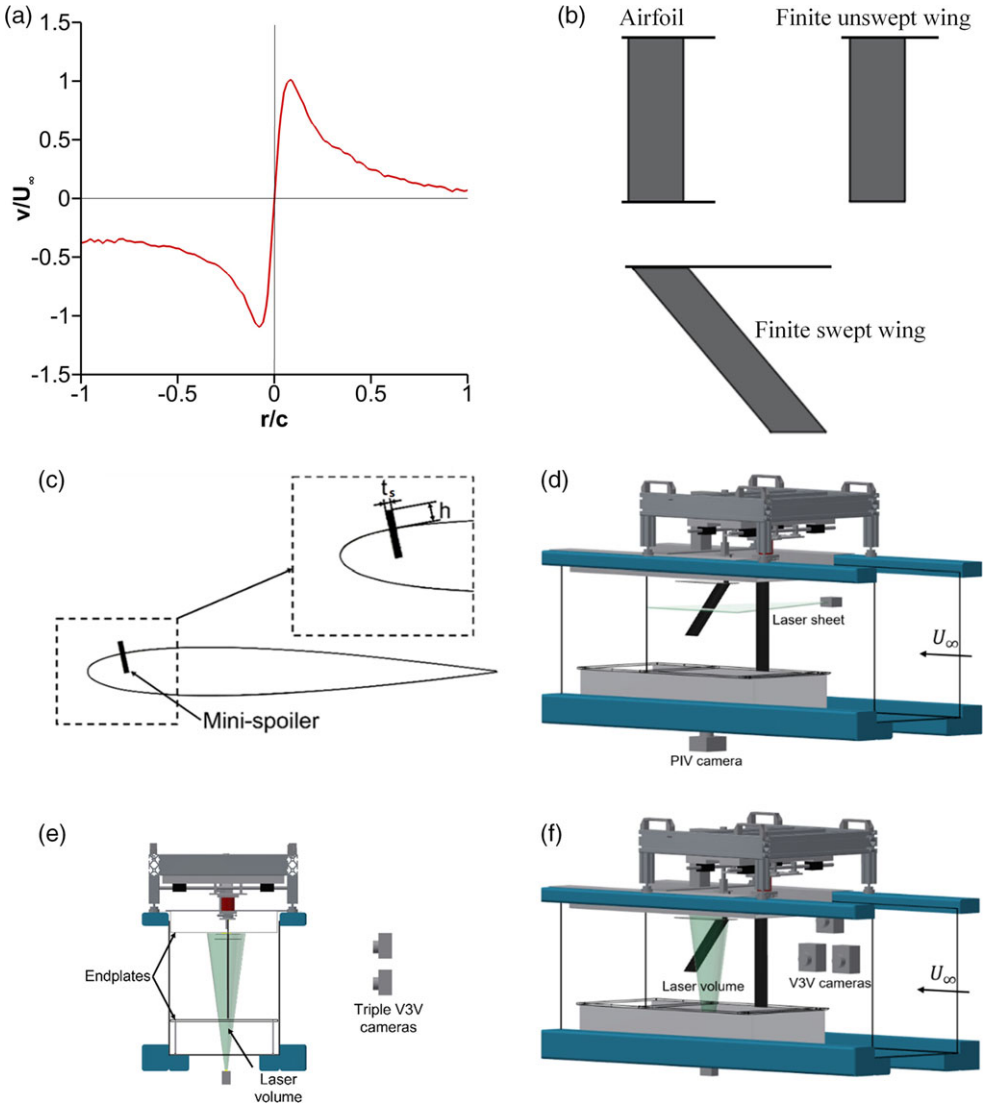

Figure 1. *Experimental setup showing (a) variation of vortex tangential velocity; (b) three aerofoil/wing models tested; (c) geometry of mini-spoiler; (d) PIV measurements (isometric view); (e) upstream view of the test section; (f) volumetric velocity measurements (isometric view).*

The geometry of the mini-spoiler is illustrated in Fig. 1(c). For the size and location of the mini-spoiler, we followed our previous studies [25, 26, 35]. The mini-spoiler was placed perpendicularly to the wing surface at $x = 0.08c$ from the leading edge in the chordwise direction. It had a height of $h = 0.04c$ and a thickness of $t_s = 0.013c$.

Volumetric velocity measurements as well as two-dimensional particle image velocimetry (PIV) measurements were carried out. In Fig. 1, parts (d), (e) and (f) illustrate the setup for both types of measurements. The volumetric velocity measurements use the V3V system (TSI), which includes a double-pulsed laser (ND: YAG 200 mJ, repetition rate 3.75 Hz) and three 4MP CCD cameras with Nikkor 50 mm f/1.8D lenses. In the present study, four separate volumes were used for the swept wing cases and two volumes were used for the unswept wing. The data for multiple volumes were collected

https://doi.org/10.1017/aer.2023.26 Published online by Cambridge University Press

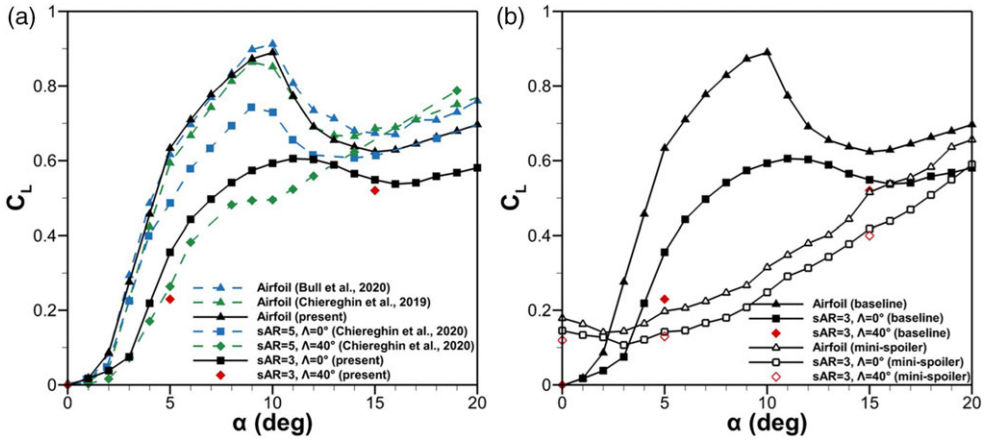

Figure 2. *Lift coefficient as a function of angle of attack in freestream for: (a) aerofoil, unswept wing and swept wing, and comparison with literature at Re = 20,000; (b) comparison of lift coefficient with and without mini-spoiler.*

separately and then the volumes were merged by using reference points on the wing or aerofoil. The volumetric measurements in this setup had a spatial resolution of 6.4%c with an uncertainty of around 3%U_∞. The advantage of three-dimensional three-component velocity measurements is balanced by a poor spatial resolution. In contrast, the PIV spatial resolution was around 2.5%c and the uncertainty was 2%U_∞ in the experiments. Figure 1(d) shows the setup for the particle image velocimetry (PIV) measurements. The PIV system uses the same double-pulsed laser (ND: YAG 200 mJ, repetition rate 3.75 Hz) and an 8MP Powerview Plus CCD camera with a Nikkor 50 mm f/1.8D lens. The comparison and discussion of the two methods were presented in Qian et al. [19]. The advantages and disadvantages of the two methods necessitate the complementary use of both of them. For both methods, a total of 60 image pairs were taken for each selected phase to calculate the phase-averaged flows.

Lift force measurements were conducted for the gust-wing interactions with and without mini-spoiler (baseline) cases. A single component binocular type load cell was utilised to measure the lift force on the downstream wing. For each experiment, force data were acquired at a sampling frequency of 2,000 Hz for the total duration and then averaged from 20 cycles. The measurement uncertainty is estimated as 5%. Figure 2(a) shows the variation of the lift coefficient with angle of attack in freestream (in the absence of the gust) for the aerofoil, unswept and swept wings. Also, the aerofoil case was compared with the literature [35, 42]. For the finite wing cases, we could not find any previous study with $sAR = 3$ and $Re = 20{,}000$. However, the available data for $sAR = 5$ at the same Reynolds number [43] are included to show the trend for the effect of aspect ratio. Figure 2(b) compares the aerofoil and the two wings with and without the mini-spoiler. The lift alleviation for all wings is substantial except for very small angle of attack (less than 2 degrees). At the very low angles of attack, including at zero angle of attack, the mini-spoiler-induced separated flow produces more lift on the upper surface, resulting in an increase in the total lift. There is also the possibility of reattachment of the separated flow at the very low angles of attack as observed in our previous studies. Except for low angles of attack, we think that the Reynolds number effect is small. This is because the current method relies on forced flow separation near the leading edge, after which the flow remains separated. It is different from the attached flows for which boundary layers may be laminar or turbulent. Even in this case, the most noticeable effect is usually the stall angle. For mini-spoilers placed near the leading edge, the magnitude of the lift reduction in the present manuscript for $Re = 20{,}000$ is similar to that for $Re = 660{,}000$ in Reference [25]. As the flow separation is fixed at the mini-spoiler, the flow transition is likely to occur in the shear layer separated from the spoiler. The closest analogy is with the plunging clean aerofoils which exhibit transitional flow at a chord Reynolds number of 10,000 [44].

https://doi.org/10.1017/aer.2023.26 Published online by Cambridge University Press

3.0 Results and discussion

The unsteady lift measurements for the downstream aerofoil and wings were carried out as a function of the offset distance between the vortex and the leading edge of the aerofoil/wing and the angle of attack. For the aerofoil case, only two-dimensional PIV measurements were carried out in the mid-span plane. For the unswept wing, both the 2D-PIV measurements at the mid-span (in order to compare with the aerofoil case) and the volumetric measurements for the whole wing (in order to understand the wing-tip effects) were carried out. For the swept wing, we only performed volumetric measurements.

Figure 3 shows the vorticity fields with streamlines for the aerofoil case, and the normalised offset distance $\varepsilon = 0.6$, $\alpha = 0^\circ$, the weak vortex $\Gamma/U_\infty c = 0.55$, the baseline aerofoil (left column) and with the mini-spoiler (right column). The normalised offset distance is defined as $\varepsilon = (y_{VI} - y_{LE})/c$. Here, y_{VI} is the initial cross-stream location of the vortex at $U_\infty t/c = 2$ when the vortex rollup appears to be complete. The leading edge of the wing has the cross-stream coordinate of y_{LE}. At $t = 0$ the plunge motion of the upstream aerofoil (not in the field of view) starts and the counter-clockwise vortex enters the measurements volume from left at $U_\infty t/c = 2$. The incident vortex travels downstream over the aerofoil without significant change in the trajectory for this angle of attack and the offset distance. Despite of relatively weak interaction between the vortex and the aerofoil, the diffusion of the incident vortex when it is above the wing and the wake is apparent. This generic observation for all wings and related flow physics has been discussed by Qian et al. [19].

Even at $U_\infty t/c = 0$ (corresponding to the freestream conditions) significant flow separation due to the mini-spoiler is evident, whereas there is only weak flow separation for the baseline aerofoil throughout the gust interaction. The flow separation and the shear layer induced by the mini-spoiler appears to be stable until after the vortex passes the aerofoil when the row of small vortices have formed. Next, we examine how the interaction between the vortex and the aerofoil is affected by the aerofoil angle of attack.

3.1 Effect of angle of attack of aerofoil

The vorticity fields with streamlines are shown for $\alpha = 10^\circ$ in Fig. 4 and for $\alpha = 15^\circ$ in Fig. 5. The other parameters are the same as in Fig. 3 for $\alpha = 0^\circ$ ($\varepsilon = 0.6$ and $\Gamma/U_\infty c = 0.55$). We note that the static stall angle is approximately 10° for the baseline aerofoil. In Fig. 4, there is already a weak separation over the baseline aerofoil in freestream ($U_\infty t/c = 0$). As the incident vortex approaches and passes over the baseline aerofoil, the flow separation region has a similar size. There is even an indication of temporary reattachment at the last instant due to the downwash of the incident vortex. However, the mini-spoiler-induced flow separation is much more pronounced for $\alpha = 10^\circ$. The flow separation region does not show significant variations as the incident vortex approaches and passes. Only after the vortex has passed the aerofoil, the instability of the shear layer becomes apparent, exhibiting a row of small vortices.

For the post-stall angle of attack of $\alpha = 15^\circ$, the baseline aerofoil placed in freestream has massively separated flow (see top image in Fig. 5). In this figure, $U_\infty t/c = 0$ corresponds to the case of the aerofoil in steady freestream (with no gust). For all $U_\infty t/c$, the phase-averaged flow is shown in Fig. 5. As the incident vortex approaches and passes there are significant changes in the separated flow. As the induced velocity of the approaching vortex increases, it initially reduces the separated region, causing deflection of the separated shear layer downwards at $U_\infty t/c = 2$. At later times the induced velocity near the leading edge increases the flow angle and the separated region becomes larger, eventually causing the shedding of multiple vortices. The first LEV develops and sheds while forming a couple with the incident vortex followed by the shedding of a second LEV. In contrast, the separated region over the aerofoil with the mini-spoiler is remarkably stable until after the vortex has passed the aerofoil. This may be due to the fixed separation caused by the mini-spoiler in this case. Overall, the flow fields are more stable with the mini-spoiler and thus less lift variation may be expected during the interaction.

Qian et al. [19] have shown that a positive lift peak is observed for all wings when the incident vortex is still upstream, regardless of the angle of attack and the offset distance, hence regardless of whether flow separation takes place or not. The positive peak occurs when the incident vortex reaches just upstream

https://doi.org/10.1017/aer.2023.26 Published online by Cambridge University Press

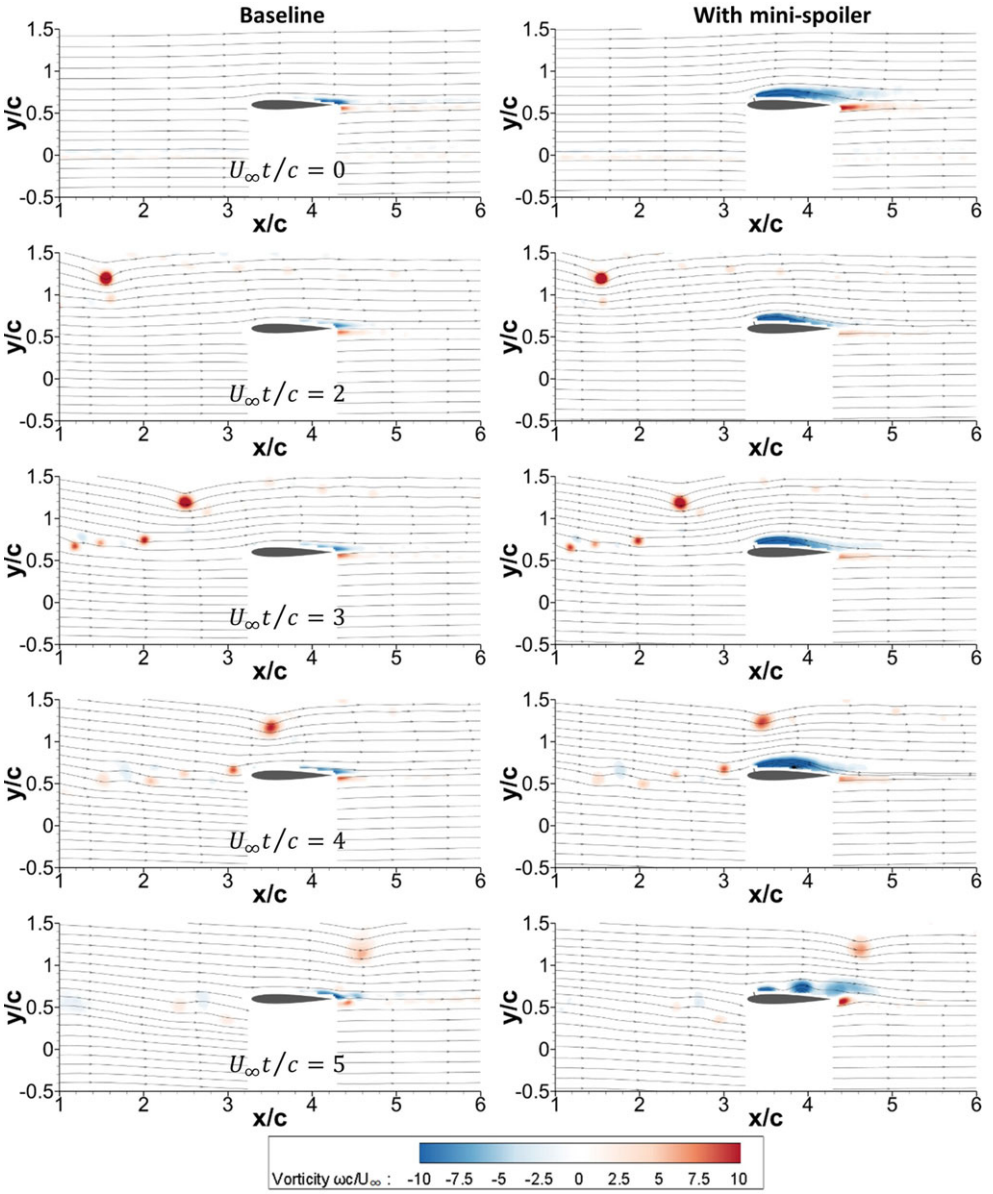

Figure 3. *Vorticity field with streamlines for the baseline aerofoil (left column) and with mini-spoiler (right column) for weak vortex* $\Gamma/U_\infty c = 0.55$, $\varepsilon = 0.6$, $\alpha = 0°$.

of the wing (roughly 30%c) at around $U_\infty t/c = 3.5$. This distance corresponds to approximately five vortex core radii from the leading edge. The variation of the unsteady lift coefficient for the baseline aerofoil and with the mini-spoiler are shown in Fig. 6 at $\alpha = 0°$, 5°, 10°, and 15°, for $\Gamma/U_\infty c = 0.55$ and $\varepsilon = 0.6$ (corresponding to the cases in Figs. 3 to 5). (Note that parts (a) and (b) have the same scale, but the vertical axis is shifted according to the range of the values.) The positive peaks also occur around the same instant $U_\infty t/c = 3.5$ with the mini-spoiler at all angles of attack. This confirms that the mini-spoiler induced separation region does not have a significant effect on the arrival time of the incident vortex. The maximum lift coefficient is reduced with the mini-spoiler, except for $\alpha = 0°$. The

https://doi.org/10.1017/aer.2023.26 Published online by Cambridge University Press

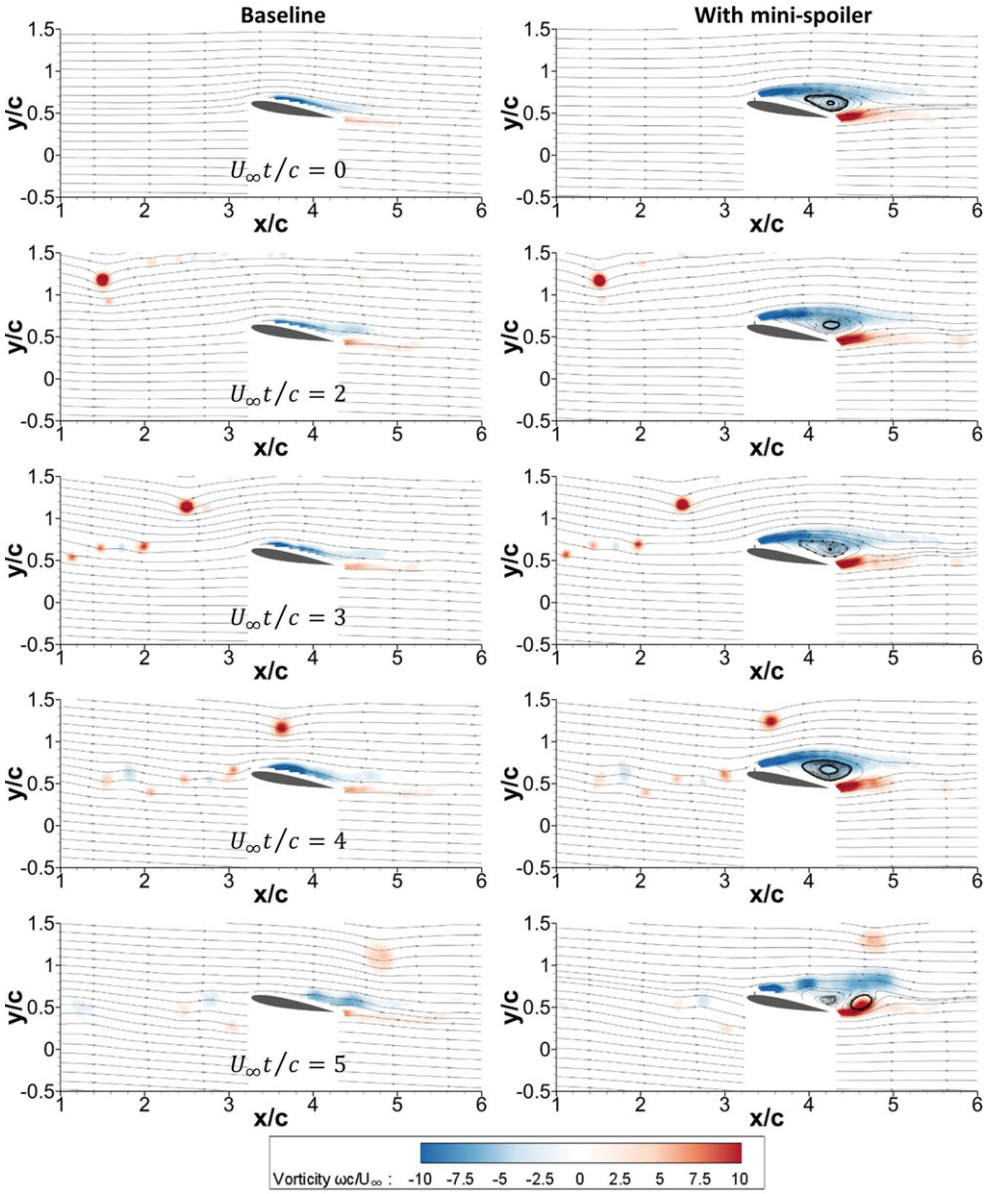

Figure 4. *Comparison of vorticity fields between baseline aerofoil (left column) and with mini-spoiler (right column) for* $\Gamma/U_\infty c = 0.55$, $\varepsilon = 0.6$, $\alpha = 10^\circ$.

maximum lift reduction appears to be for the stall angle of $\alpha = 10^\circ$. For each angle of attack, there is also a minimum lift, which may have a broader peak. The minimum lift is reached around $U_\infty t/c = 5$. It is seen in Figs. 3–5 that at this instant the incident vortex is downstream of the trailing edge. The downwash of the incident vortex may also cause flow separation on the lower surface and a long recovery time for the unsteady lift [19]. Nevertheless, the important quantity for loads attenuation is the positive peak lift force for a loaded wing.

The effect of the normalised offset distance ε on the maximum lift for the baseline aerofoil has been discussed by Qian et al. [19] in detail. The induced velocity in the cross-stream direction and the effective

https://doi.org/10.1017/aer.2023.26 Published online by Cambridge University Press

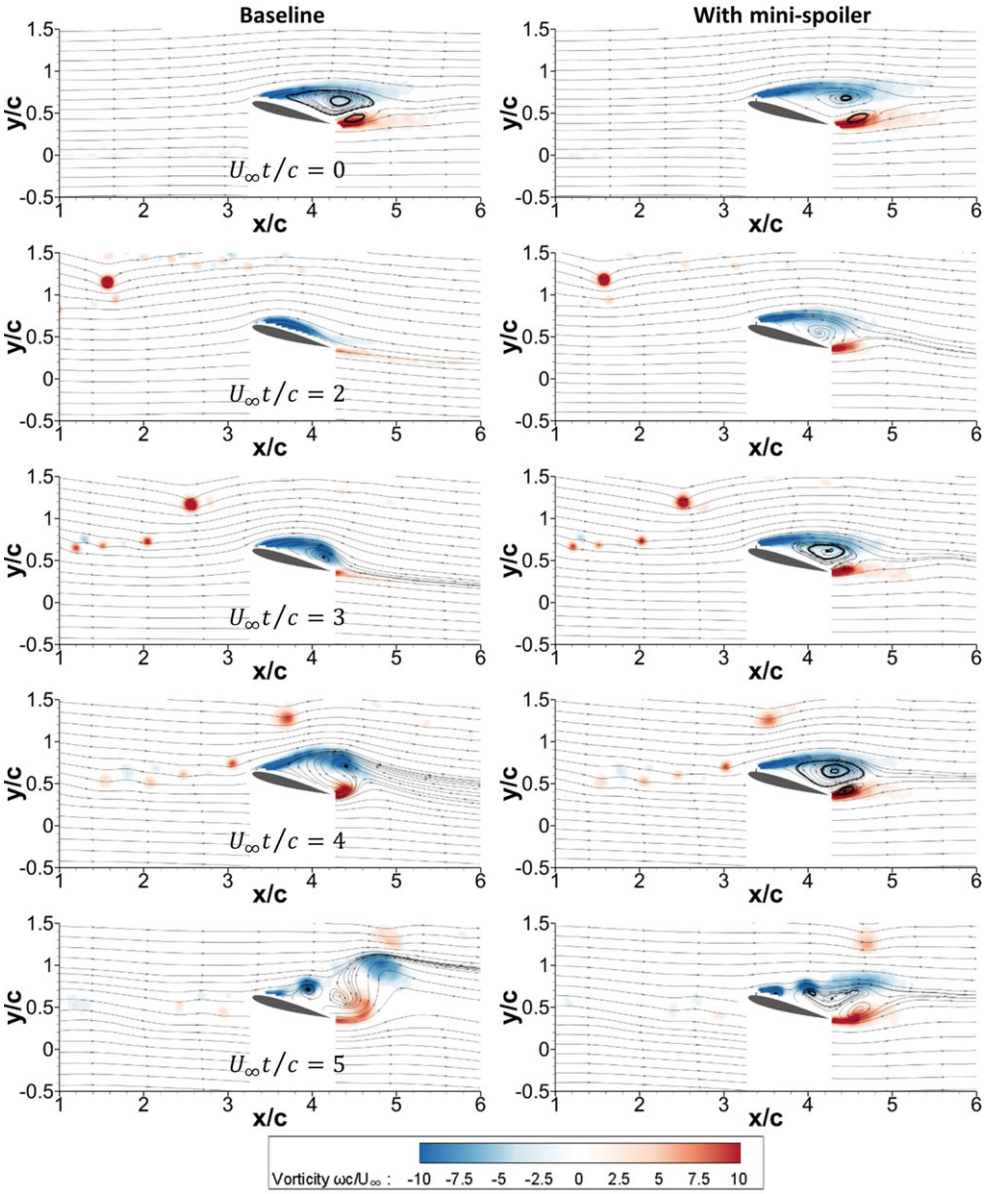

Figure 5. *Comparison of vorticity fields between baseline aerofoil (left column) and with mini-spoiler (right column) for* $\Gamma/U_\infty c = 0.55$, $\varepsilon = 0.6$, $\alpha = 15°$.

angle of attack both increase as the incident vortex approaches. If the interaction is assumed to be quasi-steady, a simple reduced order model [19] predicts that the induced velocity by the incident vortex on the wing becomes maximum for the head-on collision ($\varepsilon = 0$). The previous experiments and the data in Fig. 7 reveal that there is a slight asymmetry. Such asymmetric effects for the baseline aerofoil, which were also reported by Peng and Gregory [18], can be explained by the accelerated flow on the wing surface for $\varepsilon > 0$ and decelerated flow on the lower surface for $\varepsilon < 0$. The positive peak lift for the aerofoil with the mini-spoiler also exhibits similar variations to that of the baseline aerofoil. For all offset distances tested, there is an increase in the peak lift coefficient for $\alpha = 0°$, but a decrease for the pre-stall

https://doi.org/10.1017/aer.2023.26 Published online by Cambridge University Press

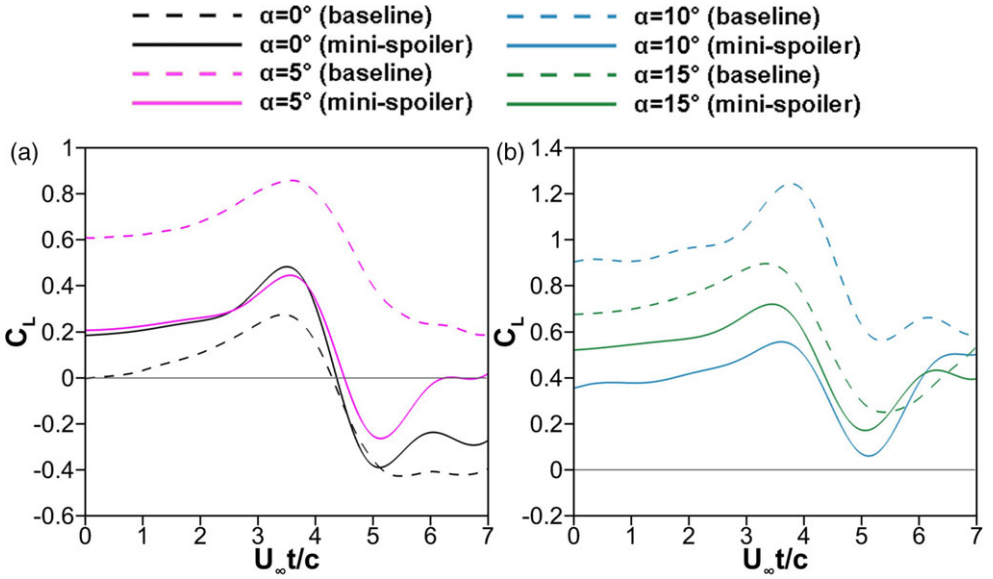

Figure 6. *Lift time history for baseline aerofoil and with mini-spoiler for* $\Gamma/U_\infty c = 0.55$, $\varepsilon = 0.6$ *at: (a)* $\alpha = 0°$ *&* $5°$, *(b)* $\alpha = 10°$ *&* $15°$.

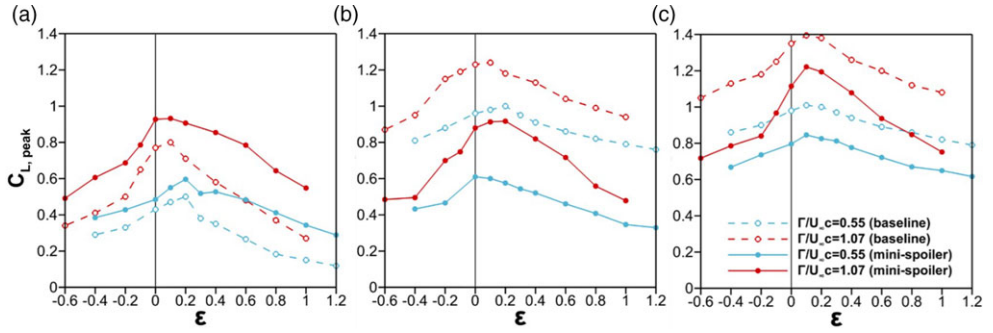

Figure 7. *Peak coefficient of lift for the baseline aerofoil and with mini-spoiler for (a)* $\alpha = 0°$, *(b)* $\alpha = 5°$, *(c)* $\alpha = 15°$.

angle of attack of $\alpha = 5°$ and the post-stall angle of attack of $\alpha = 15°$. In general, the lift reduction is better for the pre-stall angle of attack. In contrast, there is already stalled flow for the baseline aerofoil at the post-stall angle of attack. There is also some influence of the offset distance. For the post-stall angle of attack ($\alpha = 15°$), there is a degraded performance of the mini-spoiler for the strong vortex at small offset distances ($\varepsilon = 0$ to 0.2). For these conditions, the flow over the baseline aerofoil may be massively separated, making further lift reduction with the mini-spoiler small.

The effectiveness of the mini-spoiler can be quantified as the change in the peak lift coefficient:

$$\Delta C_{L,peak} = C_{L,\ mini-spoiler,\ peak} - C_{L,\ baseline,\ peak}$$

The variation of the quantity $\Delta C_{L,peak}$ is shown as a function of aerofoil angle of attack in Fig. 8 for the weak vortex $\Gamma/U_\infty c = 0.55$. We note that, as given in Section 2, the maximum tangential velocity V_{max}/U_∞ is approximately 0.5 (the variation of the tangential velocity of the vortex as a function of distance from the centre is given by Qian et al. [19]). The maximum tangential velocity can be considered

https://doi.org/10.1017/aer.2023.26 Published online by Cambridge University Press

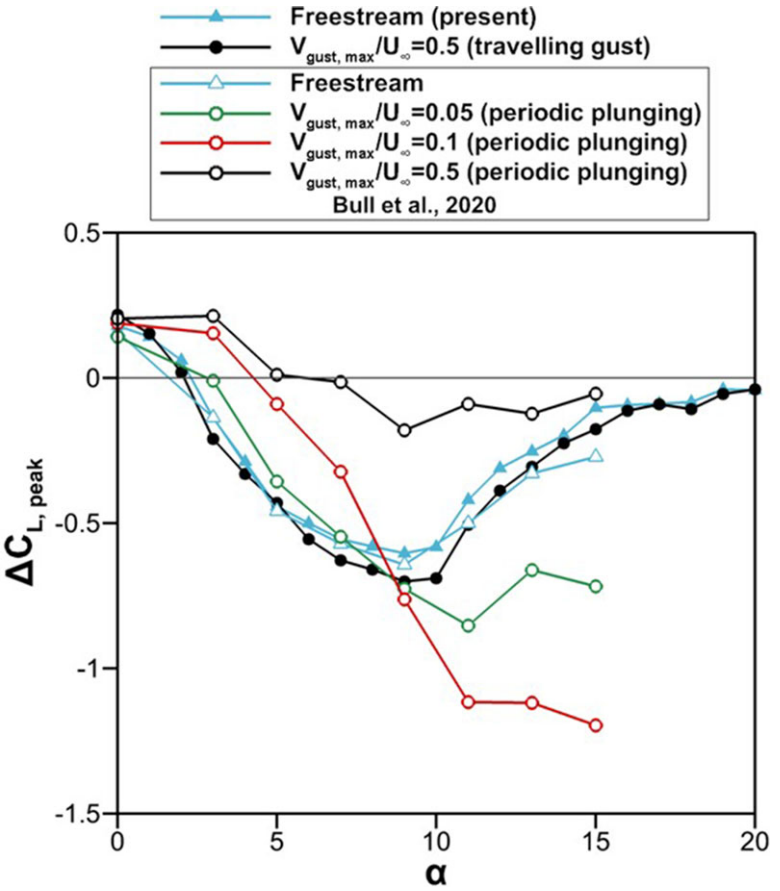

Figure 8. *Variation of change in peak coefficient of lift $\Delta C_{L,\,peak}$ as a function of angle of attack for travelling vortical gust ($\Gamma/U_\infty c = 0.55$, $\varepsilon = 0.6$) and periodic plunging motion.*

as the maximum gust velocity in our case, i.e. $V_{gust,\,max}/U_\infty = 0.5$. In Fig. 8 this case is shown as "travelling gust" with black solid circles. We also present the change in the lift coefficient in the freestream (in the absence of the gust). It is interesting that the change in the lift coefficient of the mini-spoiler on the aerofoil placed in steady freestream is almost identical to that when it is placed in the travelling gust. It may appear paradoxical that the mini-spoiler causes the same changes in the lift when in freestream and in the gust, even though the absolute values of the lift coefficient are significantly affected by the gust. We note that the positive peak of the lift force appears to be quasi-steady in nature as discussed above and modelled by Qian et al. [19].

It will be interesting to compare the effectiveness of the spoiler in the travelling vortical gust and in the plunging motion previously studied [35]. The latter also represents the limiting case of infinite wavelength of a travelling transverse gust. For the case of the plunging aerofoil, the equivalent maximum gust velocity is taken as the maximum plunge velocity. The data calculated from Bull et al. [35] for various values of $V_{gust,\,max}/U_\infty$ are shown in Fig. 8. When the travelling gust is compared with the plunging aerofoil for the same value of $V_{gust,\,max}/U_\infty = 0.5$, the changes in the lift coefficient are vastly different. The mini-spoiler does not appear to be effective over the whole range of angle of attack for the plunging aerofoil. (This can be attributed to the formation of the strong LEVs for both the baseline case and with the mini-spoiler, which makes the mini-spoiler inefficient.) However, for much lower values of plunge (or equivalently, gust) velocity, the effectiveness of the mini-spoiler on the plunging aerofoil

https://doi.org/10.1017/aer.2023.26 Published online by Cambridge University Press

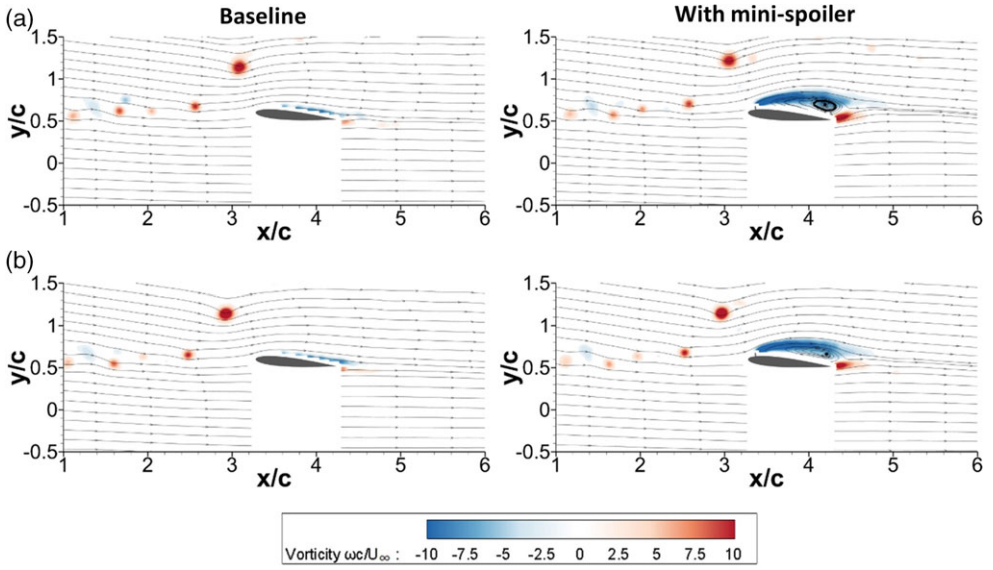

Figure 9. *Vorticity fields at $U_\infty t/c = 3.5$ for baseline aerofoil (left column) and with mini-spoiler (right column) for (a) aerofoil, (b) finite unswept wing, $\Gamma/U_\infty c = 0.55$, $\varepsilon = 0.6$, $\alpha = 5°$.*

increases and may even exceed the static effectiveness at the post-stall angle of attack (the mechanism of this superior performance was discussed by Bull et al. [35]). It is noted that, for the plunging aerofoil, the transverse velocity acts on the whole chord length of the aerofoil simultaneously. In contrast, the travelling gust in our experiments has the maximum gust velocity only for a small region around the vortex core (the core radius is about $0.06c$ for the travelling vortex). It appears that the length scale of the unsteadiness has significant influence on the effectiveness of the spoiler.

3.2 Effect of wing aspect ratio

The vorticity fields with streamlines at $U_\infty t/c = 3.5$ are compared for the loaded aerofoil in part (a) and for the finite unswept wing in part (b), with and without the mini-spoiler, in Fig. 9 for $\alpha = 5°$, $\Gamma/U_\infty c = 0.55$, and $\varepsilon = 0.6$. The PIV measurements were carried out in the mid-span plane for both the aerofoil and the wing. We note that the peak positive lift is observed around this instant for the aerofoil case. The flow fields for the aerofoil and the finite wing look very similar at this instant. The only noticeable difference is the streamwise location of the incident vortex. For the finite unswept wing, the incident vortex is slightly delayed. In Fig. 9, we see approximately the same shift in the streamwise location of the incident vortex between the upper row (aerofoil) and the lower row (finite wing). The shift/delay is roughly the same for the baseline case (left column) and with the spoiler (right column). This may be due to the smaller strength of the bound vortex of the finite wing compared to that of the aerofoil. The bound vortex, which has a clockwise direction, is expected to induce velocity on the incident vortex and accelerate it as the two become closer. We suggest that the delay of the incident vortex for the finite wing is due to the weaker bound vortex for the finite wing. This is consistent with the reduced effective angle of attack of the finite wing due to the aspect ratio correction.

This is supported by the time history of the lift coefficient shown in Fig. 10. The variations of the lift coefficient for the aerofoil and the finite wing are similar, exhibiting positive peaks around the same time, but appear to be scaled down. Qian et al. [19] presented a simple prediction of the maximum lift based on the lifting line theory for the steady aerodynamics. This quasi-steady approach provided a reasonable approximation. Figure 10 shows that, in the presence of the mini-tab, the variation of the

https://doi.org/10.1017/aer.2023.26 Published online by Cambridge University Press

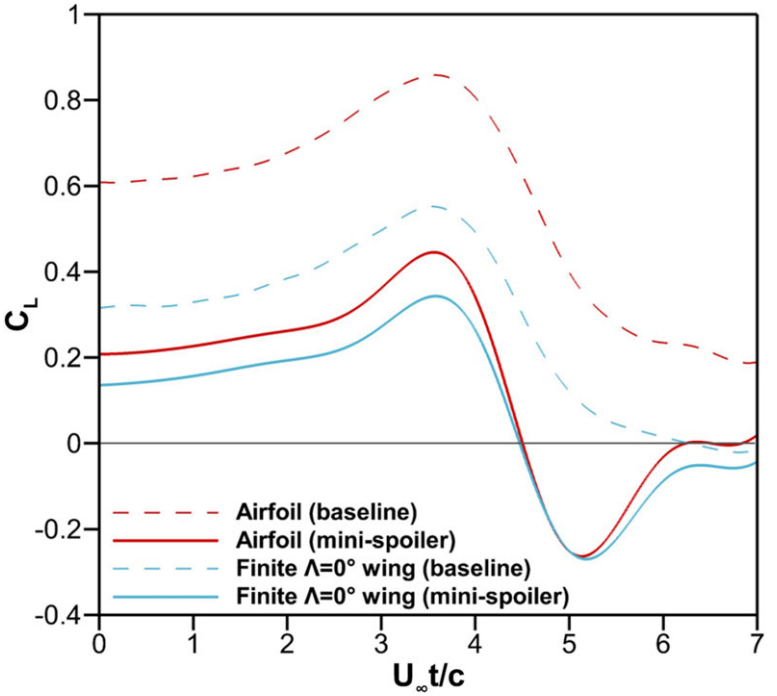

Figure 10. *Time history of lift coefficient of aerofoil and finite $\Lambda = 0°$ wing, with and without mini-spoiler, for $\Gamma/U_\infty c = 0.55$, $\varepsilon = 0.6$ at $\alpha = 5°$.*

lift coefficient with the mini-spoiler is also similar for the positive lift; however, negative lift peaks are observed, which may be due to the flow separation on the lower surface. Overall, the reduced positive lift for the finite wing is consistent with the reduced effective angle of attack.

The change in the maximum lift coefficient $\Delta C_{L,peak}$ for the aerofoil and the wing, in the freestream and in the travelling gust, is shown in Fig. 11 as a function of angle of attack for $\Gamma/U_\infty c = 0.55$ and $\varepsilon = 0.6$. The variations of the change in the maximum lift coefficient are similar for the aerofoil and the wing, exhibiting the best lift reduction around the stall angle. The magnitudes for the finite wing appear to be smaller by a constant factor, which is related to the reduced effective angle of attack. We made a prediction for the change in the lift coefficient of the finite wing by using the data for the aerofoil and making a correction for the aspect ratio. We used the Prandtl's lifting line theory with the assumption of an elliptical circulation variation:

$$\frac{C_{L,3D}}{C_{L,2D}} = \frac{1}{1 + \frac{a_0}{\pi AR}}$$

and the slope of the lift coefficient was taken from the thin aerofoil theory (because of the non-linearity in the experiments shown in Fig. 2). The prediction is also shown in Fig. 11 with the dashed line, which reveals an excellent agreement with the measured data for the finite wing up to the stall angle. In this region, for both the aerofoil and the wing, the effectiveness of the mini-spoiler in the gust is slightly better than that in the freestream.

The volumetric velocity measurements were compared in Fig. 12 for the finite unswept wing at $\alpha = 10°$, with and without the mini-spoiler, $\Gamma/U_\infty c = 0.55$ and $\varepsilon = 0.6$. At the stall angle of attack, the effectiveness of the mini-spoiler for the aerofoil and the wing differs most (see Fig. 11). We studied this angle of attack to investigate any interactions between the incident gust and the wing-tip vortex, and possible effect on the wing flow. In Fig. 12, the iso-surfaces of $Q^* = Qc^2/U_\infty^2 = 5$ are shown at $U_\infty t/c = 4$ and $U_\infty t/c = 4.5$. The iso-surfaces are coloured by the spanwise vorticity ($\omega c/U_\infty$). The

https://doi.org/10.1017/aer.2023.26 Published online by Cambridge University Press

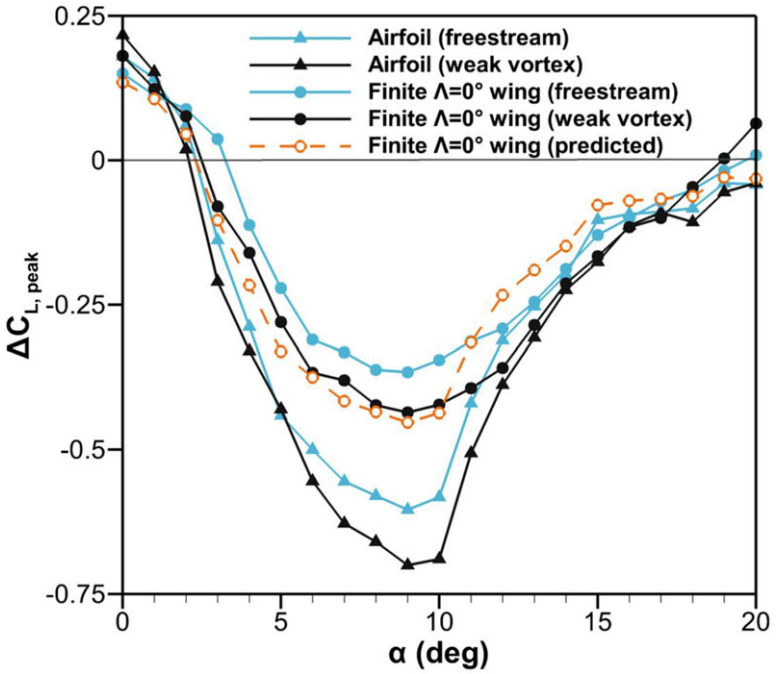

Figure 11. *Change in lift coefficient $\Delta C_{L,peak}$ as a function of angle of attack for aerofoil and finite unswept wing in freestream and in gust, $\Gamma/U_\infty c = 0.55$, $\varepsilon = 0.6$.*

incident vortex remains nearly two-dimensional as it travels over the wing. There is no evidence of any influence of the wingtip and tip vortex on the incident vortex for this offset distance. However, the effect of the wingtip is visible for the baseline wing case shown in Fig. 12(a) for $U_\infty t/c = 4$. The leading-edge vortex shed from the wing is anchored at the wingtip, while the inboard part remains parallel to the leading edge but slightly downstream of the incident vortex. (We note similar shapes of the leading-edge vortex filaments on plunging wings at high reduced frequencies [45]) In contrast, for the wing with the mini-spoiler, there is no evidence of roll-p of a coherent LEV shedding at the same instant. Instead, the separated shear layer appears disorganised. In other words, the mini-spoiler prevents the rollup of the vortices. This feature is similar to that observed for wings plunging at not-so-high frequencies [35]. In Fig. 12(b) for $U_\infty t/c = 4.5$, the leading-edge vortices just upstream and just downstream of the incident vortex are visible for the mini-tab case.

In Fig. 13 for $U_\infty t/c = 4$, the iso-surfaces of $Q^* = Qc^2/U_\infty^2 = 5$ are coloured by the spanwise velocity w/U_∞ (the positive velocity is towards the wingtip). There is no significant spanwise flow in the incident vortical gust during the interaction for both the baseline wing and with the mini-spoiler. There is some spanwise flow near the root towards the tip, but it becomes very weak as the wingtip region is approached. Outboard of the wingtip in the freestream there is a slight spanwise flow towards the wing root. However, in the leading-edge vortex (for the baseline wing) and in the separated shear flow (for the wing with the mini-spoiler), there is no sign of any spanwise flow.

3.3 Effect of wing sweep

Qian et al. [19] have shown that the measured maximum lift coefficient can be estimated using the independence principle unless gust interaction produces a leading-edge vortex at post-stall angles of attack. Hence, volumetric velocimetry measurements were performed on the finite swept wing interacting with the strong vortex $\Gamma/U_\infty c = 1.07$, at an offset distance $\varepsilon = 0.4$ and $\alpha = 15°$. Figures 14–16 present the

https://doi.org/10.1017/aer.2023.26 Published online by Cambridge University Press

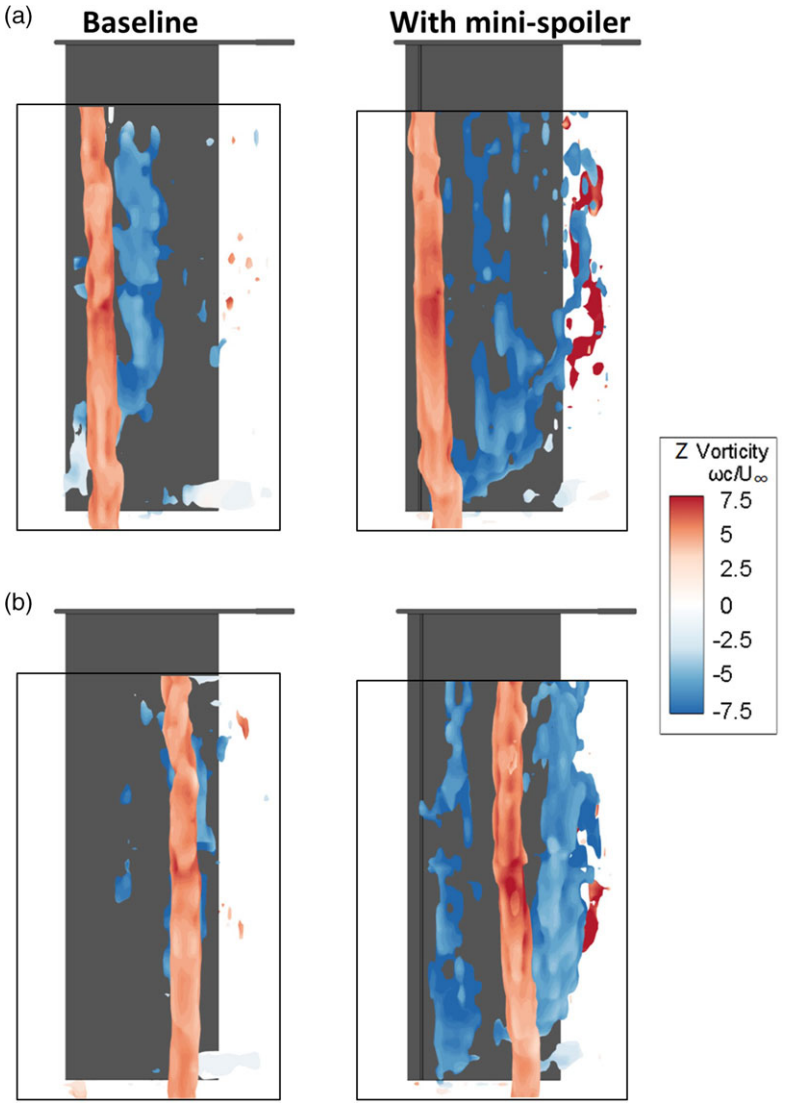

Figure 12. *Isosurfaces of Q^*=5 coloured by z-vorticity ($\omega c/U_\infty$) for baseline and with mini-spoiler for finite $\Lambda = 0°$ wing at (a) $U_\infty t/c = 4$; (b) $U_\infty t/c = 4.5$; $\Gamma/U_\infty c = 0.55$, $\varepsilon = 0.6$, $\alpha = 10°$.*

iso-surfaces $Q^* = 5$ coloured by the spanwise vorticity during the vortex interaction at $U_\infty t/c = 3$ (Fig. 14), $U_\infty t/c = 4$ (Fig. 15), and $U_\infty t/c = 5$ (Fig. 16), with the top views (top) and the three-dimensional views (bottom).

At $U_\infty t/c = 3$, there is already flow separation from the wing, which forms a coherent leading-edge vortex. The angle of the axis of the leading-edge vortex is slightly larger than the wing sweep angle. However, with the mini-spoiler, the flow separation appears disorganised at this instant. When the incident vortex is roughly in the mid-span region at $U_\infty t/c = 4$, the leading-edge vortex becomes nearly parallel to the wing leading edge for the baseline wing as it sheds and convects with the incident vortex. In contrast, with the mini-spoiler, the flow separation is organised as a leading-edge vortex that is nearly parallel to the incident vortex. At the final stage of $U_\infty t/c = 5$, the incident vortex is highly three-dimensional and partly diffused for both cases. The inboard part of the incident vortex filament

https://doi.org/10.1017/aer.2023.26 Published online by Cambridge University Press

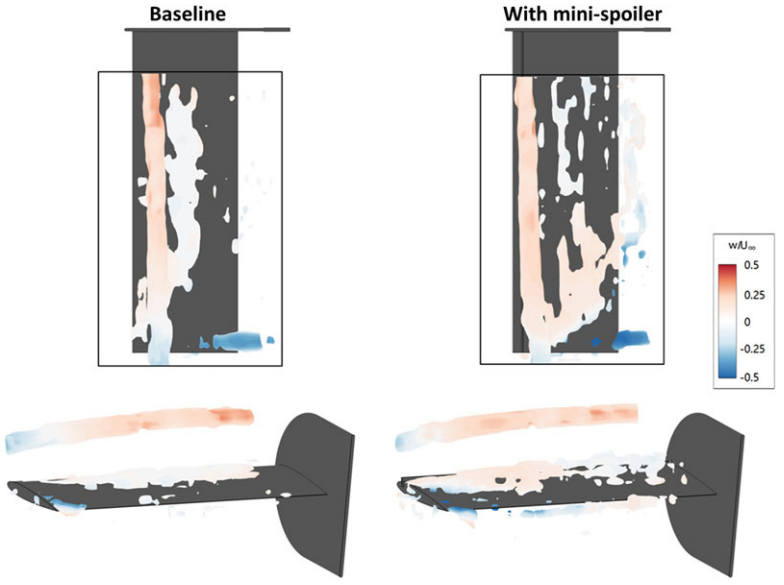

Figure 13. *Isosurfaces of Q^*=5 coloured by spanwise velocity (w/U_∞) for baseline finite $\Lambda = 0°$ wing and with mini-spoiler at $U_\infty t/c = 4$, for $\Gamma/U_\infty c = 0.55$, $\varepsilon = 0.6$, $\alpha = 10°$.*

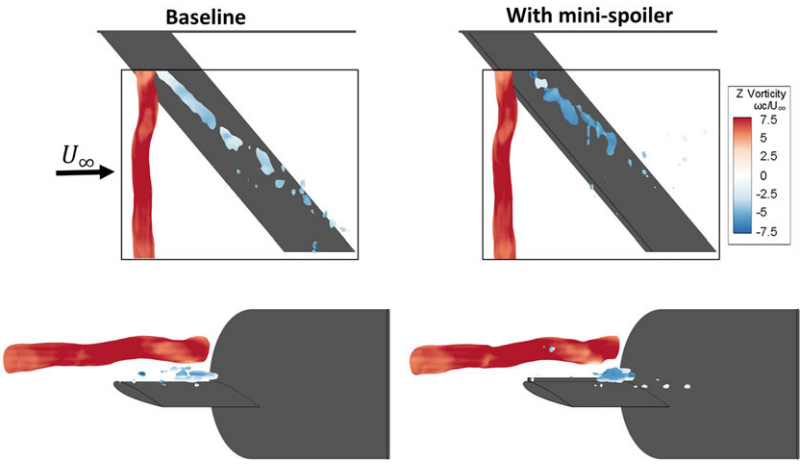

Figure 14. *Isosurfaces of Q^*=5 coloured by z-vorticity ($\omega c/U_\infty$) for baseline and with mini-spoiler for strong vortex $\Gamma/U_\infty c = 1.07$, finite $\Lambda = 40°$ wing, $\varepsilon = 0.4$, $\alpha = 15°$ at $U_\infty t/c = 3$.*

is already downstream of the wing and exhibits large three-dimensional distortion. Consequently, the leading-edge vortex is also three-dimensional and further away from the wing surface.

For the same case, the isosurfaces of $Q^* = 5$, 35, 50, 70 in Fig. 17 are coloured by the spanwise velocity w/U_∞ along the z-axis in the incident vortex and the velocity w'/U_∞ along the wing sweep angle elsewhere. For both definitions of the velocity components, the positive velocity is towards the wingtip. There is negligible spanwise flow in the incident vortex upstream of the wing and during the interaction with the wing, for both the baseline wing and with the mini-spoiler. On the wing, there is strong flow along the axis of the leading-edge vortex, especially in the inboard part of the vortex filament,

https://doi.org/10.1017/aer.2023.26 Published online by Cambridge University Press

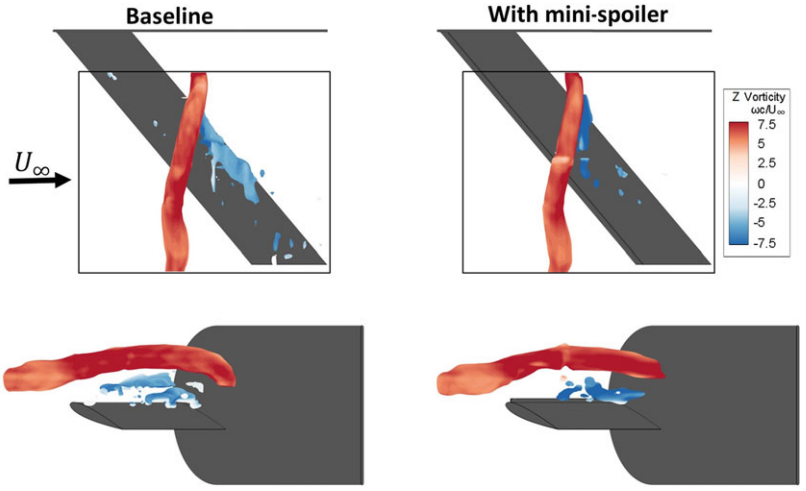

Figure 15. *Isosurfaces of Q^*=5 coloured by z-vorticity ($\omega c/U_\infty$) for baseline and with mini-spoiler for strong vortex $\Gamma/U_\infty c = 1.07$, finite $\Lambda = 40^\circ$ wing, $\varepsilon = 0.4$, $\alpha = 15^\circ$ at $U_\infty t/c = 4$.*

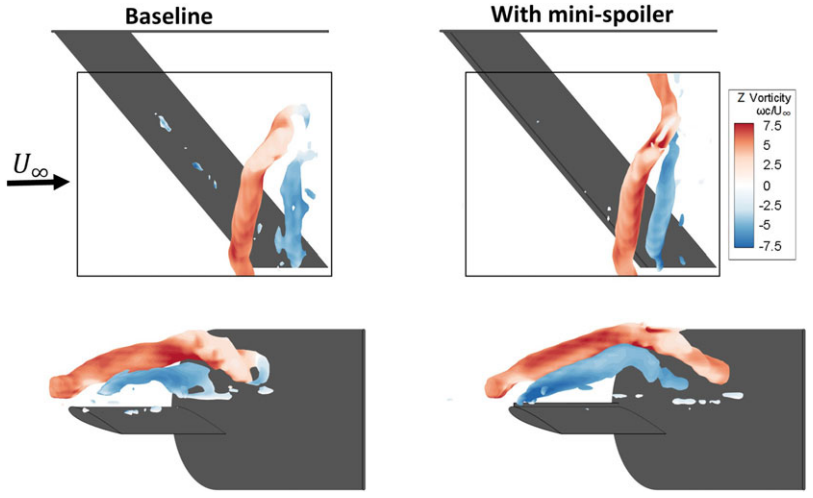

Figure 16. *Isosurfaces of Q^*=5 coloured by z-vorticity ($\omega c/U_\infty$) for baseline and with mini-spoiler for strong vortex $\Gamma/U_\infty c = 1.07$, finite $\Lambda = 40^\circ$ wing, $\varepsilon = 0.4$, $\alpha = 15^\circ$ at $U_\infty t/c = 5$.*

for the baseline wing. The vortex gradually becomes nearly parallel to the wing sweep. With the mini-spoiler, initially we do not observe strong flow along the wing. However, strong spanwise flow develops as the incident vortex moves over the wing, while becoming nearly parallel to the incident vortex.

For the unswept and the swept wing at the same angle of attack and in the same gust case as in Fig. 17, the time history of the lift coefficient is compared in Fig. 18 for the baseline case and with the mini-spoiler. Compared to the unswept wing case, the swept wing has smaller peak lift and slower increase and slower decrease of the wing lift as also demonstrated by [19]. This is due to the delayed arrival time of the incident vortex as it approaches the outboard sections of the wing, resulting in asynchronous sectional lift and smaller total lift. Again, there is not much difference in the pattern of the lift coefficients and timings of the peaks. The mini-spoiler can reduce the maximum lift, whereas there is not much influence for the minimum (negative) lift.

https://doi.org/10.1017/aer.2023.26 Published online by Cambridge University Press

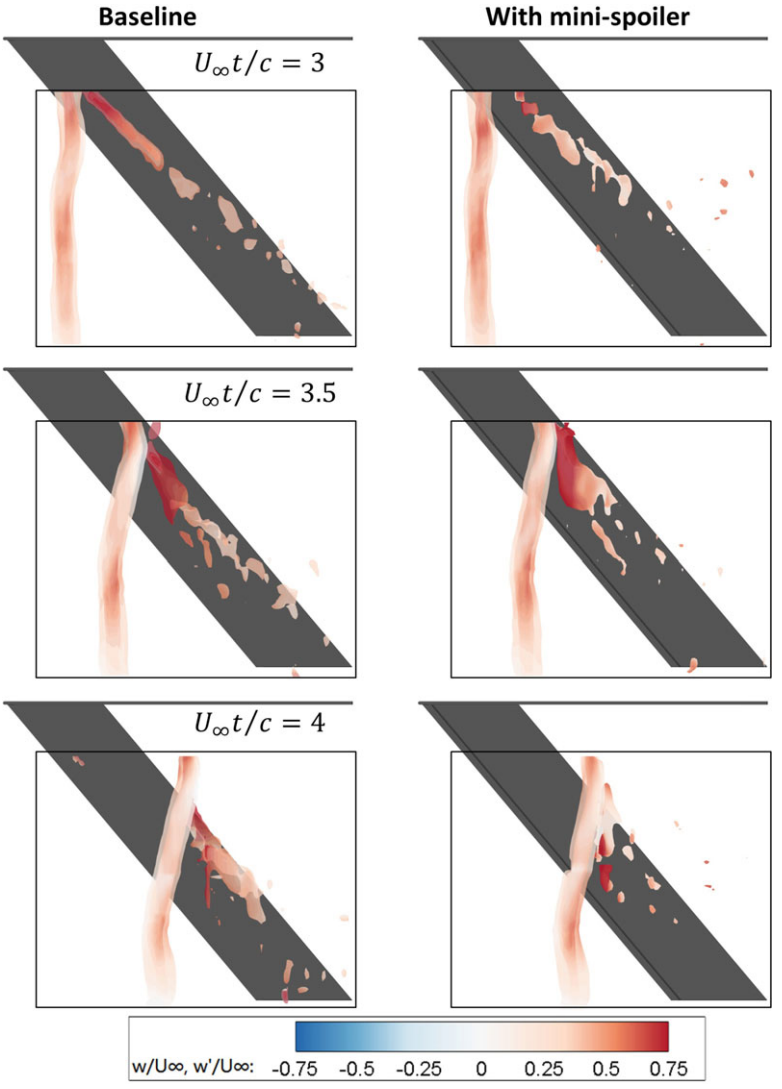

Figure 17. *Isosurfaces of Q^*=5, 35, 50, 70 coloured by velocity in z-direction (w/U_∞) and spanwise velocity (w'/U_∞) for baseline and with mini-spoiler for strong vortex $\Gamma/U_\infty c = 1.07$, finite $\Lambda = 40^\circ$ wing, $\varepsilon = 0.4$, $\alpha = 15^\circ$.*

The effect of the wing sweep is illustrated in Fig. 19 by comparing the peak lift coefficients for the swept and the unswept wing cases at the same post-stall angle of attack ($\alpha = 15^\circ$). It is concluded that the effectiveness of the mini-spoiler on the swept wing is not sensitive to either the strength of the incident vortex or the offset distance within the range tested. This may be due to the lessening effect of the asynchronous viscous interaction and flow separation for small offset distances. In contrast, for the unswept wing (Fig. 19(a)), the effectiveness exhibits some degradation for the interaction of the strong vortex with small offset, which implies that substantial flow separation is taking place simultaneously in the spanwise direction for the baseline case and making the spoiler ineffective for the already separated flow. On the other hand, the mini-spoiler effectiveness is generally better for the unswept wing except for the strongest vortex-wing interactions.

https://doi.org/10.1017/aer.2023.26 Published online by Cambridge University Press

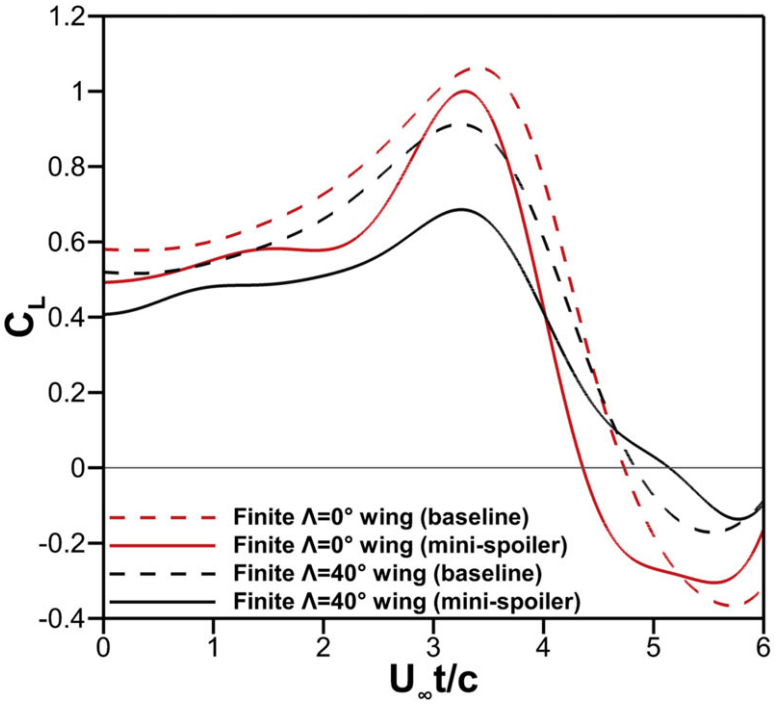

Figure 18. *For swept and unswept wings, time history of lift coefficient for baseline and with mini-spoiler,* $\Gamma/U_\infty c = 1.07$*, finite wing* $\Lambda = 40°$*,* $\varepsilon = 0.4$*,* $\alpha = 15°$*.*

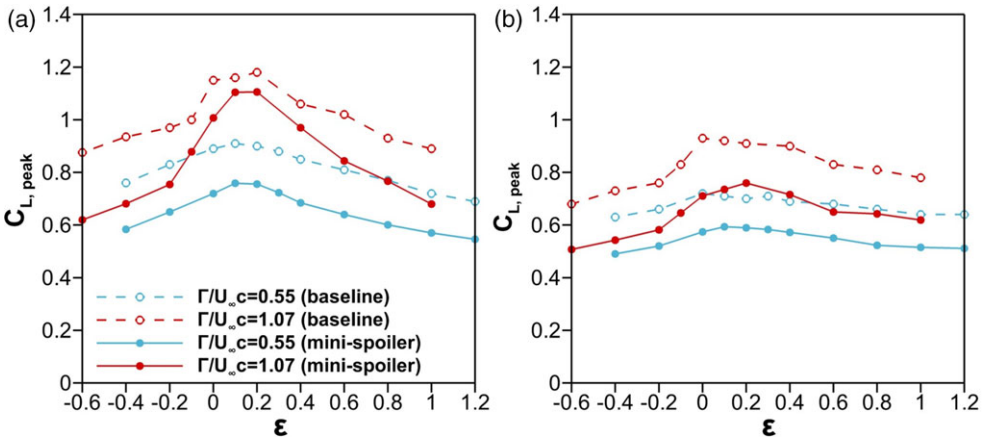

Figure 19. *Peak lift coefficient for baseline and with mini-spoiler at* $\alpha = 15°$*, for (a)* $\Lambda = 0°$*, (b)* $\Lambda = 40°$*.*

4.0 Conclusions

Lift alleviation on aerofoils, unswept and swept wings in a single isolated vortical gust was investigated. The nearly two-dimensional vortical gusts were generated by plunging an upstream aerofoil, and their interaction with stationary wings were studied by force and velocity measurements in water tunnel experiments. Aiming for the fixed-wing applications, for which the main objective is to reduce the maximum lift force and bending moment, mini-spoilers (with a height of 4% of the chord-length) placed near the

https://doi.org/10.1017/aer.2023.26 Published online by Cambridge University Press

leading edge were explored during the gust-wing interaction. Such devices are known to be effective in steady freestream and on plunging aerofoils, however, their effectiveness has not been previously studied in travelling gusts.

For pre-stall angles of attack, flow separation region and shear layer induced by the mini-spoiler are little affected during the gust encounter until after the vortex passes the aerofoil. This holds for the post-stall angle of attack as well. After the incident vortex passes, shear layer instability and formation of a row of vortices are observed. In contrast, the flow over the baseline aerofoil during the gust encounter can undergo large changes from nearly attached flows to massively separated flows. The unsteady lift for the baseline aerofoil as well as with the mini-spoiler exhibits a peak around the same instant and before the incident vortex arrives near the leading edge. The mini-spoiler can reduce the maximum lift, except for very small angles of attack. The maximum lift reduction occurs for the static stall angle of attack. For the post-stall angles of attack, the lift reduction capability rapidly decreases. This is due to the already separated flow of the baseline aerofoil near the leading edge at post-stall angles of attack. In this case, the mini-spoiler becomes ineffective. Surprisingly, for the whole range of angles of attack, the change in the lift coefficient by the mini-spoiler is almost the same when in steady freestream and in travelling gust. For the same identical maximum gust velocity, which is around 50% of the freestream velocity, the mini-spoiler appears to lose its effectiveness for plunging aerofoils as reported by a previous study. This is due to the effectively infinite wavelength for the plunging aerofoil compared to the gust in our experiments, which has a finite length scale. We conclude that the length scale of the incident vortex has a profound influence on the effectiveness of the mini-spoiler.

For the finite wing-gust encounter, the three-component volumetric measurements reveal that the incident vortex filament remains as two-dimensional and that there is no significant spanwise flow. The flow separation and the LEV shed from the baseline wing are affected by the presence of the wingtip and the LEV resembles LEVs over moving wings. In contrast, the mini-spoiler prevents the formation of a coherent vortex. The unsteady lift of the finite wing during the gust encounter is similar to that of the aerofoil, exhibiting positive peaks around the same time but with different magnitude due to the reduced effective angle of attack. Again, the best lift reduction is found to be around the stall angle. The magnitude of the lift reduction can be estimated using the aerofoil data and by making an aspect ratio correction.

For the swept wing at a post-stall angle of attack, the approaching incident vortex may induce formation of a leading-edge vortex in the baseline case. This LEV may have significant spanwise flow. The mini-spoiler prevents the formation of a coherent leading-edge vortex along the wing span. There is no spanwise flow in the incident vortex during the encounter. With the mini-spoiler, at later stages a vortex parallel to the incident vortex may develop from the separated shear layer and may also have strong spanwise flow. The mini-spoiler can reduce the maximum lift; however, its effectiveness for the swept wing is smaller than that of the unswept wing.

We only measured the lift force in this study. It is envisaged that mini-spoilers near the leading- edge will be used for loads attenuation during extreme loads in gust encounters. A temporary drag increase due to the activated mini-spoiler is considered to be unimportant compared to the main objective of the protecting wing structure. For the full-span spoilers studied in this paper, we have not measured bending moment. However, bending moment reduction during extreme loads will be the main objective for part-span spoilers. For this more realistic case, other aerodynamic features such as changes in the total pitching moment of the wing should be investigated.

Acknowledgements. The authors acknowledge the support of Airbus in an advisory role for this project and thank Dr. Andrea Castrichini for valuable discussions.

References

[1] Heathcote, D.J. *Aerodynamic load alleviation using minitabs*, PhD Thesis, University of Bath, U.K., 2017.
[2] Gursul, I. Vortex flows on UAVs: Issues and challenges, *Aeronaut. J.*, 2004, **108**, (1090), pp 597–610.
[3] Theodorsen, T. General theory of aerodynamic instability and the mechanism of flutter, NACA-TR-496, 1949.

https://doi.org/10.1017/aer.2023.26 Published online by Cambridge University Press

[4] Sears, W.R. Some aspects of non-stationary airfoil theory and its practical application, *J. Aeronaut. Sci.*, 1941, **8**, (3), pp 104–108.
[5] Cordes, U., Kampers, G., Meißner, T., Tropea, C., Peinke, J. and Hölling, M. Note on the limitations of the Theodorsen and Sears functions, *J. Fluid Mech.*, 2017, **811**, R1.
[6] Wei, N.J., Kissing, J., Wester, T.T., Wegt, S., Schiffmann, K., Jakirlic, S., Holling, M., Peinke, J. and Tropea, C. Insights into the periodic gust response of airfoils, *J. Fluid Mech.*, 2019, **876**, pp 237–263.
[7] Fernandez, F., Cleaver, D. and Gursul, I. Unsteady aerodynamics of a wing in a novel small-amplitude transverse gust generator, *Exp. Fluids*, 2021, **62**, (1), pp 1–20.
[8] McCroskey, W.J. Unsteady airfoils, *Annu. Rev. Fluid Mech.*, 1982, **14**, (1), pp 285–311.
[9] Gilman Jr, J. and Bennett, R.M. A wind-tunnel technique for measuring frequency-response functions for gust load analyses, *J. Aircr.*, 1966, **3**, (6), pp 535–540.
[10] Booth Jr, E.R. and Yu, J.C. Two-dimensional blade-vortex flow visualization investigation, *AIAA J.*, 1986, **24**, (9), pp 1468–1473.
[11] Wilder, M.C. and Telionis, D.P. Parallel blade–vortex interaction, *J. Fluids Struct.*, 1998, **12**, (7), pp 801–838.
[12] Brion, V., Lepage, A., Amosse, Y., Soulevant, D., Senecat, P., Abart, J.C. and Paillart, P. Generation of vertical gusts in a transonic wind tunnel, *Exp. Fluids*, 2015, **56**, (7), pp 1–16.
[13] Wei, N.J., Kissing, J. and Tropea, C. Generation of periodic gusts with a pitching and plunging airfoil, *Exp. Fluids*, 2019, **60**, (11), pp 1–20.
[14] Wu, Z., Bangga, G., Lutz, T., Kampers, G. and Hölling, M. Insights into airfoil response to sinusoidal gusty inflow by oscillating vanes, *Phys. Fluids*, 2020, **32**, (12), p 125107.
[15] Jones, W.P. and Moore, J.A. Flow in the wake of a cascade of oscillating airfoils, *AIAA J.*, 1972, **10**, (12), pp 1600–1605.
[16] Bicknell, J. and Parker, A. A wind-tunnel stream oscillation apparatus, *J. Aircr.*, 1972, **9**, (6), pp 446–447.
[17] Peng, D. and Gregory, J.W. Vortex dynamics during blade-vortex interactions, *Phys. Fluids*, 2015, **27**, (5), p 053104.
[18] Peng, D. and Gregory, J.W. Asymmetric distributions in pressure/load fluctuation levels during blade-vortex interactions, *J. Fluids Struct.*, 2017, **68**, pp 58–71.
[19] Qian, Y., Wang, Z. and Gursul, I. Interaction of quasi-two-dimensional vortical gusts with airfoils, unswept and swept wings, *Exp. Fluids*, 2022, **63**, (8), pp 1–25.
[20] Wooding, C.L. and Gursul, I. Unsteady aerodynamics of low aspect ratio wings at low Reynolds numbers, *Royal Aeronautical Society Aerospace Aerodynamics Research Conference*, London, June 2003.
[21] Holmes, D.W. Lift and measurements in an aerofoil in unsteady flow, *Turbo Expo Power Land Sea Air*, 1973, **79801**,break p V001T01A041.
[22] Yen Nakafuji, D.T., van Dam, C.P., Michel, J. and Morrison, P. Load control for turbine blades: a non-traditional microtab approach, *Wind Energy Symp.*, 2002, **7476**, pp 321–330.
[23] Baker, J.P., Standish, K.J. and van Dam, C.P. Two-dimensional wind tunnel and computational investigation of a microtab modified airfoil, *J. Aircr.*, 2007, **44**, (2), pp 563–572.
[24] Cooperman, A.M., Chow, R. and van Dam, C.P. Active load control of a wind turbine airfoil using microtabs, *J. Aircr.*, 2013, **50**, (4), pp 1150–1158.
[25] Heathcote, D.J., Gursul, I. and Cleaver, D.J. Aerodynamic load alleviation using minitabs, *J. Aircr.*, 2018, **55**, (5), pp 2068–2077.
[26] Heathcote, D.J., Gursul, I. and Cleaver, D.J. Dynamic deployment of a minitab for aerodynamic load control, *J. Aircr.*, 2020, **57**, (1), pp 41–61.
[27] Blaylock, M., Chow, R., Cooperman, A. and van Dam, C.P. Comparison of pneumatic jets and tabs for active aerodynamic load control, *Wind Energy*, 2014, **17**, (9), pp 1365–1384.
[28] Al-Battal, N.H., Cleaver, D.J. and Gursul, I. Lift reduction by counter flowing wall jets, *Aerosp. Sci. Technol.*, 2018, **78**, pp 682–695.
[29] Al-Battal, N.H., Cleaver, D.J. and Gursul, I. Unsteady actuation of counter-flowing wall jets for gust load attenuation, *Aerosp. Sci. Technol.*, 2019, **89**, pp 175–191.
[30] Tan, Y. and Glezer, A. Bi-directional control of airfoil's aerodynamic loads at low angles of attack using fluidic actuation, *AIAA Scitech 2019 Forum*, San Diego, California, January 2019, p 0889.
[31] Li, Y. and Qin, N. Airfoil gust load alleviation by circulation control, *Aerosp. Sci. Technol.*, 2020, **98**, p 105622.
[32] Li, Y. and Qin, N. Gust load alleviation by normal microjet, *Aerosp. Sci. Technol.*, 2021, **117**, p 106919.
[33] Kearney, J. and Glezer, A. Aero-effected flight control using distributed active bleed, *41st AIAA Fluid Dynamics Conference and Exhibit*, Honolulu, Hawaii, June 2011, p 3099.
[34] DeSalvo, M., Heathcote, D., Smith, M.J. and Glezer, A. Direct lift control using distributed aerodynamic bleed, *AIAA SciTech 2019 Forum*, San Diego, California, January 2019, p 0591.
[35] Bull, S., Chiereghin, N., Cleaver, D.J. and Gursul, I. Novel approach to leading-edge vortex suppression, *AIAA J.*, 2020, **58**, (10), pp 4212–4227.
[36] Corke, T.C. and Thomas, F.O. Dynamic stall in pitching airfoils: Aerodynamic damping and compressibility effects, *Annu. Rev. Fluid Mech.*, 2015, **47**, pp 479–505.
[37] Greenblatt, D. and Wygnanski, I. Dynamic stall control by periodic excitation, part 1: NACA 0015 parametric study, *J. Aircr.*, 2001, **38**, (3), pp 430–438.
[38] Greenblatt, D., Nishri, B., Darabi, A. and Wygnanski, I. Dynamic stall control by periodic excitation, part 2: Mechanisms, *J. Aircr.*, 2001, **38**, (3), pp 439–447.

https://doi.org/10.1017/aer.2023.26 Published online by Cambridge University Press

[39] Karim, M.A. and Acharya, M. Suppression of dynamic-stall vortices over pitching airfoils by leading-edge suction, *AIAA J.*, 1994, **32**, (8), pp 1647–1655.
[40] Post, M.L. and Corke, T.C. Separation control using plasma actuators: dynamic stall vortex control on oscillating airfoil, *AIAA J.*, 2006, **44**, (12), pp 3125–3135.
[41] Visbal, M.R. and Garmann, D.J. Mitigation of dynamic stall over a pitching finite wing using high-frequency actuation, *AIAA J.*, 2020, **58**, (1), pp 6–15.
[42] Chiereghin, N., Cleaver, D.J. and Gursul, I. Unsteady lift and moment of a periodically plunging airfoil, *AIAA J.*, 2019, **57**, (1), pp 208–222.
[43] Chiereghin, N., Bull, S., Cleaver, D.J. and Gursul, I. Three-dimensionality of leading-edge vortices on high aspect ratio plunging wings, *Phys. Rev. Fluids*, 2020, **5**, (6), p 064701.
[44] Cleaver, D.J., Wang, Z., Gursul, I. and Visbal, M.R. Lift enhancement by means of small-amplitude airfoil oscillations at low reynolds numbers, *AIAA J.*, 2011, **49**, (9), pp 2018–2033.
[45] Son, O., Gao, A.K., Gursul, I., Cantwell, C.D., Wang, Z. and Sherwin, S.J. Leading-edge vortex dynamics on plunging airfoils and wings, *J. Fluid Mech.*, 2022, **940**, A28.

Cite this article: Qian Y., Wang Z. and Gursul I. (2023). Lift alleviation in travelling vortical gusts. *The Aeronautical Journal*, **127**, 1676–1697. https://doi.org/10.1017/aer.2023.26